Heart Rate Variability with Photoplethysmography in 8 Million Individuals: Results and Scaling Relations with Age, Gender, and Time of Day

Aravind Natarajan,[1*] Alexandros Pantelopoulos,[1] Hulya Emir-Farinas,[1] Pradeep Natarajan[2,3,4]

[1]Fitbit Research, 199 Fremont St, Fl #14, San Francisco, CA 94105, USA
[2]Center for Genomic Medicine and Cardiovascular Research, Massachusetts General Hospital, Boston, MA 02114, USA
[3]Department of Medicine, Harvard Medical School, Boston, MA 02115, USA
[4]Program in Medical and Population Genetics, Broad Institute of Harvard & MIT, Cambridge, MA 02142, USA

[*]To whom correspondence should be addressed; E-mail: anatarajan@fitbit.com

Heart rate variability, or the variation in the time interval between consecutive beats, is a non-invasive dynamic metric of the autonomic nervous system and an independent risk factor for cardiovascular death. Prior limitations of use include requirements for continuous electrocardiography and lack of reference standards. Consumer wrist-worn tracking devices using photoplethysmography now provide the unique potential of continuously measuring surrogates of sympathetic and parasympathetic activity through the analysis of interbeat intervals. Here we leverage wrist-worn trackers to present the largest, to our knowledge, analysis of heart rate variability in humans across the time, frequency, and graphical domains. We derive diurnal parasympathetic and

sympathetic measures and provide scaling parameters by age, sex, and time of day. Poincare plots graphically summarize heart rate variability metrics and may detect common arrhythmias. Lastly, we observe a strong dose-dependent correlation between daily steps and optimal heart rate variability metrics. Our results provide the ability to interpret continuous heart rate variability for tens of millions of wrist-worn trackers already in use.

Introduction

Heart rate variability (HRV) refers to the variation in time between successive heart beats, and represents a non-invasive index of the autonomic nervous system. Since the autonomic nervous system regulates heart rate during sinus rhythm, HRV summarizes complex non-linear cardiovascular accommodative responses, dictated by the parasympathetic and sympathetic nervous systems, to dynamic physiologic variations.

While HRV is significantly influenced by sex and aging (*1*), reduced compensatory response (i.e., low HRV) is independently predictive of first fatal and non-fatal cardiovascular disease events in the general population (*2–6*). Robust data also links low HRV with adverse outcomes and mortality after sustaining a cardiovascular event, such as myocardial infarction (*7, 8*). Beta-blockers and exercise therapy reduce risks of cardiovascular events among individuals with coronary artery disease and congestive heart failure, and enhancement of HRV is believed to be mechanisms for improved prognosis (*9–11*). Thus, a less adaptive autonomic nervous system is predictive of first and recurrent cardiovascular events, and restoration of homeostatic capacity may reduce risk.

A recent position statement from professional societies lament a general disconnect between HRV as a research tool and practical clinical use (*12*). Among the barriers for clinical use, include assessments in relatively small selected cohorts, requirement for continuous ECG

monitoring, and substantial variation by age, sex, and time of day.

In recent years, the widespread availability of heart rate enabled tracking devices has caused considerable interest in HRV given potential ease of availability. Commercial wrist-worn tracking devices measure heart rate intervals through photoplethysmography (PPG) at a single point of contact. PPG devices uses multiple wavelengths of light to illuminate the skin and photodiodes to measure the reflected light, thereby inferring changes in blood volume by measuring changes in light absorption (see for e.g. (*13–15*)). While ECG-derived HRV metrics are obtained by analyzing the RR intervals between successive beats, PPG devices resolve HRV metrics through analysis of interbeat intervals (IBI) as a proxy for the RR intervals (*16–19*). PPG devices are more susceptible to motion artifacts.

Standards for HRV were set by the European Society of Cardiology, and the North American Society of Pacing and Electrophysiology (*20, 21*). HRV can be measured in many ways: in the time domain, the frequency domain, or using graphical and non-linear techniques (for an overview of HRV and metrics, see (*22*)). In this article, we present time domain, frequency domain, and graphical domain results from the largest HRV study to-date by several orders of magnitude - from $\sim$ 8 Million users of Fitbit devices. We demonstrate feasibility of obtaining HRV metrics from PPG at high fidelity, define diurnal distributions of common HRV metrics by age and sex, characterize the influence of aging on HRV metrics, and the relationship between physical activity on HRV metrics.

Data and HRV metrics

Time domain metrics are computationally straightforward and do not require contiguous data. Frequency domain calculations can be computationally expensive and require the data to be contiguous and evenly sampled, but have the benefit of separating the sympathetic nervous system (fluctuations that occur on longer time scales and hence low frequencies) and the parasym-

pathetic nervous system (fluctuations mostly occur on shorter time scales and hence higher frequencies) (*22*). Time windows of 5 minutes (short term) and 24 hours (long term) are commonly considered in the literature (*20, 21*). In this work, we only consider 5 minute windows, i.e. a 24 hour time series would have 288 time windows. Note that 24 hour measurements of time domain metrics will be larger than the 5 minute measurements which we discuss in this work. We consider the following well known HRV metrics:

1. SDRR: The SDRR is the standard deviation of the IBI measured over a time window of 5 minutes. Let the peaks of the blood volume occur at times T_0, T_1, $T_2, \cdots$. The IBI are the differences between successive beats, defined as:

$$I_n = T_n - T_{n-1}, \tag{1}$$

   i.e. the IBI field is the first difference of the PPG waveform. The standard deviation of each 5 minute sequence of I_n is computed. The SDRR measures medium to long term variations in the heart rate. SDRR correlates with the total power since the variance in the time domain equals the total power in the frequency domain. In the literature, this quantity is often termed SDNN which implies that ectopic beats are filtered out (*22*). Since we do not do this, we prefer the term SDRR.

2. RMSSD: The RMSSD is the root mean squared (RMS) value of the successive differences of the I_n. The successive differences ΔI_n are defined as:

$$\Delta I_n = I_n - I_{n-1}. \tag{2}$$

   Since the ΔI_n is the second difference of the PPG waveform (or the first difference of the IBI), it preferentially contains high frequency variations. The RMSSD is the RMS value of the ΔI_n (i.e. the square root of the mean of the square of the samples), measured over

a time window of 5 minutes. The RMSSD measures short to medium term variations in the heart rate, and correlates with HF power.

3. LF Power: The LF band measures power in the frequency range 0.04 Hz - 0.15 Hz (corresponding to physiological processes that act on timescales 6.7s - 25s), and captures both sympathetic and parasympathetic activity. Mayer waves, i.e. arterial blood pressure waves are seen in the LF band (typically around 0.1 Hz). Some vagally mediated power may also be present in the LF band, particularly during slow, paced breathing (see for example (*22*) and references therein).

4. HF Power: The HF band measures power in the frequency range 0.15 Hz - 0.4 Hz (corresponding to physiological processes that act on timescales 2.5s - 6.7s), and is a probe of the parasympathetic nervous system. The respiration induced sinus arrhythmia is usually contained in the HF band.

5. Poincare S_1: The standard deviation measured along the minor axis of the Poincare ellipse is called S_1, and is a measure of short term variability.

6. Poincare S_2: The standard deviation measured along the major axis of the Poincare ellipse is called S_2, and is a measure of long term variability.

It is well known that respiration modulates the heart rate due to the activity of the vagus nerve, at frequencies $\approx$ the respiration rate $\sim 10 - 20$ times a minute during sleep, a phenomenon known as sinus arrhythmia (SA) (see for example (*22*) and references therein). The magnitude of the SA provides a measure of parasympathetic cardiovascular response to respiration. HRV is also a probe of sympathetic activity at lower frequencies: Mayer waves are oscillations of arterial pressure occurring spontaneously, and are enhanced during states of sympathetic activation (*23*). Fig. 1 shows the Power Spectral Density (PSD), i.e. power per unit

frequency, for a single individual, measured over one night. The PSD shows two features:

1. Peak at ≈ 0.1 Hz corresponding to the arterial blood pressure induced Mayer wave.

2. Peak at ≈ 0.3 Hz corresponding to the respiration induced sinus arrhythmia.

We fit the data to the following form:

$$\log_{10}\left(\frac{\mathrm{PSD}}{\mathrm{s}^2/\mathrm{Hz}}\right) = \left[K + \nu \log_{10}\left(\frac{f}{0.15\,\mathrm{Hz}}\right)\right] \times \left[1 + A_{\mathrm{M}} \exp -\frac{1}{2}\left(\frac{f-\mu_{\mathrm{M}}}{\sigma_{\mathrm{M}}}\right)^2 + A_{\mathrm{R}} \exp -\frac{1}{2}\left(\frac{f-\mu_{\mathrm{R}}}{\sigma_{\mathrm{R}}}\right)^2\right] \quad (3)$$

The first term represents a power law decline with frequency. The second term accounts for the two features. In this example, the best fit value for the Mayer wave is $\mu_{\mathrm{M}} = 0.0975$ Hz representing arterial pressure oscillations on a mean time scale ≈ 10.3 s. The best fit value for the SA feature for this subject was found to be $\mu_{\mathrm{R}} = 0.2879$ Hz, corresponding to a mean respiration rate ≈ 17.3 breaths per minute.

Among graphical domain techniques, we consider only first order lag-1 Poincare plots. Poincare ellipses can be categorized by their shape into a number of classes (*24–26*). Esperer et al. (*25*) investigated Poincare plots from healthy and symptomatic individuals and identified 10 distinct classes, each with diagnostic value. Some classes of Poincare ellipses obtained from our data, are shown in Fig. 2. The top row shows heart beats in sinus rhythm. (a) is the "comet class" and represents a healthy heart. (b) is termed the "torpedo" class since it lacks the taper seen in the comet plots. Tulppo et al. (*26*) distinguish the comet and torpedo classes based on the ratio of short and long axes. Esperer et al. (*25*) instead, distinguish these classes based on the HRV. The torpedo shaped Poincare plots show cardiovascular dysfunction since the short term variability is weaker than what is seen in the comet plots. (c) is an example of tachycardia, and shows very low variability with substantially reduced S_1 and S_2. The bottom row shows examples of arrhythmias. (d) shows the "fan" pattern suggestive of atrial fibrillation (*24, 25*), while

(e) and (f) show bi-lobed and tri-lobed anomalies which could potentially indicate premature atrial or ventricular beats.

Changes in HRV with age

It is well known that HRV declines with age, although the decline may be ameliorated by healthy habits, e.g. staying active, mindfulness practices, etc. Umetani et al. (*1*) studied the decline in time domain HRV metrics with age, from a dataset of 240 healthy subjects. They found that the RMSSD declines more rapidly than the SDRR (called SDNN Index in their paper). They also found that for age < 30 yr, HRV in female subjects was lower on average than in male subjects for all time domain metrics, with no gender differences for age > 50 yr. Other works that discuss HRV and aging include (*27–29*).

Fig. 3 shows the decline in HRV with aging (from age 20 yr to 60 yr), from our data. Our results are consistent with the findings of Umetani et al. (*1*) especially for measurements taken during the daytime (our SDRR corresponds to their SDNN Index). Interestingly, the decline in HRV with age depends not only on gender, but also the time of day when the measurements are made. Plots (a) and (b) show the decrease in RMSSD and SDRR respectively. The SDRR is higher on average, in men compared to women, a trend that is less noticeable with the RMSSD. Plots (c) and (d) show equivalent results for the HF power and LF power, while plots (e) and (f) show the variation in Poincare S_1 and S_2. Note that the HF power, Poincare S_1, and RMSSD behave similarly. Similarly LF power, Poincare S_2, and SDRR show a high degree of correlation. The RMSSD tends to decline faster than the SDRR, the HF power declines faster than the LF power, and the Poincare S_1 declines faster than S_2. This suggests that with increasing age, parasympathetic ability is lost sooner than sympathetic ability.

Changes in HRV with time of day

Vandewalle et al. (*30*) studied the diurnal variation of Heart Rate Variability metrics over a 24 hour period involving eight healthy male subjects, and found that HRV metrics vary throughout the day, reaching peak values in the early morning hours. Our data also shows that HRV metrics vary significantly throughout the day, and hence HRV measurements should be taken consistently at the same time of day. Fig. 4 shows the diurnal variation of HRV metrics. Plots (a) and (b) show the fractional variation of the RMSSD and the SDRR as a function of the time of day, for male (green) and female (red) subjects. Young users (age = 20-21 yr) are represented by solid lines, while older users (age = 60-61 yr) are represented by dashed lines. Plots (c) and (d) show the variation for HF power and LF power. Similarly, plots (e) and (f) show the daily modulation in S_1 and S_2. The SDRR, LF power, and Poincare S_2 show a change in phase with increase in age: Older users tend to have an earlier peak in the daily cycle, for the sympathetic measures. All HRV metrics peak early in the day ($\sim$ between 5 am and 8 am) and reach a minimum in the late evening ($\sim$ 7 pm - 8 pm).

Scaling relations

In this section, we take a closer look at the scaling of HRV with age, gender, and time of day. We parametrize the HRV by the following power law form:

$$HRV(\text{age}, g, t) = HRV_{30}(g, t) \left(\frac{\text{age}}{30\,\text{yr}} \right)^{\alpha(g,t)}, \tag{4}$$

where t is the time of day in hours from midnight, 'age' is the age in years, and g is the gender. HRV is the HRV metric being studied, which could be HF power, LF power, RMSSD, SDRR, S_1, or S_2. Note that the dependence on the time of day and the age are not separable, i.e. the power law exponent α is a function of the time of day.

The time dependance of α means that the decline in HRV with age is different at different

times of the day. Let us expand the time dependent terms in Eq. 4, i.e. HRV_{30} and α as follows:

$$\begin{aligned} HRV_{30}(g,t) &= HRV_0(g)\ [1+\delta_{\rm H}(g,t)] \\ \alpha(g,t) &= \alpha_0(g)\ [1+\delta_\alpha(g,t)] \end{aligned} \tag{5}$$

$HRV_0(g)$ and $\alpha_0(g)$ are mean values (over 24 hours) and are gender dependent. Table 1 gives the values of $\alpha_0(g)$ and $HRV_0(g)$ for the different HRV metrics. Together with the time dependent terms, one can compute the HRV given the gender, age, and time of day. Fig. 5 shows the diurnal modulation of $\delta_{\rm H}(g,t)$ and $\delta_\alpha(g,t)$. The plots for $\delta_{\rm H}(g,t)$ are sufficiently close to sinusoidal, that we can approximate $\delta_{\rm H}(g,t)$ using the first 3 Fourier components:

$$\delta_{\rm H}(g,t) = \sum_{n=1}^{3}\left[a_n(g)\ \cos\left(\frac{n\,t}{24\,{\rm hr}}\right) + b_n(g)\ \sin\left(\frac{n\,t}{24\,{\rm hr}}\right)\right]. \tag{6}$$

The values of $a_n(g)$ and $b_n(g)$ for n = 1,2,3 are tabulated in Table 2, for male and female subjects. In all cases, b_1 is the dominant term, describing a sinusoid with a period of 24 hours. The other terms are corrections to the sinusoidal variation. Tables 1 and 2 give the value of typical HRV metrics for a 30 yr old person. More accurate estimates can be obtained by accounting for the time dependent term $\delta_\alpha(t)$ as shown in Fig. 5. Typically HRV numbers for other ages can be obtained from Eq. 4, and from Tables 1 and 2.

Focusing on Fig. 5, plot (a) show the daily modulation of $\delta_{\rm RMSSD}$ (solid lines) and $\delta_{\alpha,{\rm RMSSD}}$ (dashed lines) for male (green) and female (red) subjects. Plot (b) shows the equivalent curves for the SDRR, while plots (c), (d), (e), and (f) show $\delta_{\rm H}$ and δ_α for the HF power, LF power, S_1 and S_2. The variation of $\delta_{\rm H}$ is significant in all cases. The variation of δ_α is small for HF power, significant for the RMSSD and Poincare S_1, and large for SDRR, LF power, and Poincare S_2. In light of this figure, we can better understand the phase variation seen in Fig. 4 which showed that the phase of the SDRR, LF, and S_2 modulation peaks earlier in older individuals. From Fig. 5, we note that δ_α changes rapidly when $\delta_{\rm H}$ is close to a maximum. This means that as people

get older, the SDRR/LF/S_2 at $\sim$ 7 am declines faster than the same metrics, at e.g. $\sim$ 6 am, explaining the movement of the phase with increase in age. Such as effect is not apparent in the RMSSD, HF power, or Poincare S_1 because δ_α varies slowly when $\delta_{\rm H}$ is a maximum.

Finally, we investigate the possibility of increasing HRV through behavior modification. Several authors (*31–34*) have discussed the effect of physical activity on HRV and studies have shown beneficial results. We analyzed the HRV of all participants (measured from 6 am - 7 am) grouped by the average number of steps taken per day (steps per day is averaged over a 90 day period preceding the HRV measurement). Fig. 6 shows a strong correlation between physical activity and HF and LF power (similar conclusions hold true for other metrics). Plots (a) and (b) show the change in HF and LF power respectively for younger users (ages 20-24 yr). Corresponding results for older users (ages 50-54 yr) are shown in plots (c) and (d). To estimate the impact of exercise, we modeled the HRV power variation by a linear fit: HRV power = $C + \text{steps}/\sigma$, where σ is the number of steps necessary to increase the power by 1 ms^2 on average. The values of Pearson correlation coefficient (r), C, and σ are listed in Table 3. An alternative approach to increasing HRV involves the practice of mindfulness or meditation techniques (*35–37*).

Discussion

In this article, we presented heart rate variability measurements from 8 Million individuals using Fitbit devices, taken over a period of 24 hours. We reported results on HRV metrics in the time domain, frequency domain, and the graphical domain. To compute frequency domain metrics, we first interpolated the IBI field to obtain samples that are evenly separated. The PSD was computed from the interpolated field, through a fast fourier transform. The spectral shape of the PSD of a healthy subject contains two features in addition to a power law: Respiration induced sinus arrhythmia at $\sim 0.2 - 0.3$ Hz, and the arterial blood pressure induced Mayer wave around

~ 0.1 Hz. We showed examples of Poincare plots for subjects with heart beats in sinus rhythm, as well as for subjects with arrhythmias.

We have provided benchmark tables for HRV features in the Supplementary text giving the mean, median and the $25^{\rm th} - 75^{\rm th}$ percentile ranges, for different ages, and for both male and female participants. We anticipate that a user's HRV in relation to the HRV of others of similar age and gender may be a useful feature in assessing cardiovascular risk. Popular risk assessment algorithms such as the Framingham risk score, do not take HRV into account and sometimes underestimate the risk of adverse cardiovascular events (*38*) and sometimes overestimate it (*39*). Authors (*40*) found that the Framingham risk score for men was inversely correlated with several HRV features. We are therefore optimistic that a person's HRV relative to others in their gender and age group would help improve cardiovascular risk predictions.

Our results may have important implications for the remote monitoring of human health given the widespread availability of wrist-worn trackers. First, our method allows for the continuous monitoring of autonomic and cardiovascular responses throughout life's experiences. Consistent with prior small studies, all HRV metrics decrease with age (*1, 41, 42*). The RMSSD, HF power, and Poincare S_1 decrease with age faster than the SDRR, LF power, and Poincare S_2. This suggests a more rapid decline of parasympathetic function with increasing age, compared to sympathetic activity. The LF/HF ratio shows an *increase* with age up to $\approx 50 - 60$ yr, also implying a faster decline in parasympathetic function. Prior work in older adults implies the the slope of decline in parasympathetic HRV metrics is inversely related to longevity (*42*). We also presented results showing the diurnal variation of HRV metrics. The variation is substantial, and hence it is advisable for people to interpret HRV measurements at the same time of day. With the help of this massive dataset, we have been able to show a difference between sympathetic and parasympathetic measures with respect to the phase variation of the daily modulation with age. The sympathetic measures show a phase shift towards earlier times of the day with

increase in age. Such an effect is far less noticeable with the parasympathetic measures.

Second, we presented simple formulae and tables that show how to compute typical HRV metrics from photoplethysmography for interpretation. We fitted the variation of HRV metrics with age, using a simple power law. The scaling parameters depend on gender, and time of day. The HRV metrics can be estimated given age, gender, and time of day using 2 gender dependent scaling parameters $HRV_0(g)$, $\alpha_0(g)$, and 2 gender and time dependent scaling parameters $\delta_{\rm H}(g,t)$, and $\delta_\alpha(g,t)$. The parameter $\delta_{\rm H}(g,t)$ can be well approximated using the first 3 Fourier components. The time variation of $\delta_\alpha(g,t)$ is more complicated, and we present figures that allow for quick estimations.

Third, since we observe a strong correlation between physical steps and HRV, increasing physical activity may optimize HRV metrics. While there have been other studies of exercise and HRV, they have been typically limited to small populations (*31, 32*) or to participants in a narrow age range (*33*). Due to the size of our dataset, we have been able to examine the correlation between exercise and HRV in more detail, for both young and older participants. To estimate the increase in HRV due to physical activity, we modeled the variation of HRV power with activity, by a linear approximation. The inverse slope of this curve gives us the number of additional steps per day necessary to yield a 1 ms^2 increase in power. Users of all ages may optimize their HRV through physical exercise, although the effect is larger for younger subjects, especially for HF power. The linear fit models suggest that people in the age range 20-24 yr may increase their HF power by 1 ms^2 with every $\sim$ 30 additional steps. By contrast, subjects in the age range 50-54 yr need $\sim$ 200 (female) - 300 (male) additional steps for each 1 ms^2 increase in HF power. As a result, older individuals improve their LF power more than HF power, with physical activity. Such a large difference in HF recovery with age suggests that parasympathetic function is harder to restore with physical activity, and is an important finding of the present work. While HRV metrics have been previously correlated

with cardiovascular health and mortality, our technical advance and descriptions now permit its potential use for health promotion through tens of millions of currently available wrist-worn commercial trackers. Randomized controlled trials are now necessary to demonstrate effective ways to use HRV metrics to improve health.

Acknowledgments

We thank Emily Blanchard, Eric Chang, Robert da Silva, Tony Faranesh, Karla Gleichauf, Suraj Gowda, Sarah Kernasovskiy, Belen Lafon, Lindsey Sunden, Teresa Tenfelder, and Shelten Yuen for many helpful discussions. A.N., A.P., and H. E.-F. are employees of Fitbit Inc. P.N. is supported by awards from NHLBI (R01HL142711, R01HL148050, R01HL148565) and a Hassenfeld Scholar Award from the Massachusetts General Hospital. P.N. also reports grants from Amgen, Apple, and Boston Scientific, and consulting income from Apple and Blackstone Life Sciences, all unrelated to the current work.

References

1. K. Umetani, D. H. Singer, R. McCraty, M. Atkinson, *J. Am. Coll. Cardiol.* **31**, 593 (1998).

2. S. Hillebrand, *et al.*, *Europace* **15**, 742 (2013).

3. H. Tsuji, *et al.*, *Circulation* **90**, 878 (1994).

4. J. M. Dekker, *et al.*, *Circulation* **102**, 1239 (2000).

5. V. N. Patel, *et al.*, *JACC Heart Fail* **5**, 423 (2017).

6. P. K. Stein, *et al.*, *J. Cardiovasc. Electrophysiol.* **19**, 1169 (2008).

7. R. M. Carney, *et al.*, *Arch. Intern. Med.* **165**, 1486 (2005).

8. M. T. La Rovere, *et al.*, *Circulation* **103**, 2072 (2001).

9. M. J. Niemela, K. E. Airaksinen, H. V. Huikuri, *J. Am. Coll. Cardiol.* **23**, 1370 (1994).

10. G. Malfatto, *et al.*, *Am. J. Cardiol.* **81**, 834 (1998).

11. G. Sandrone, *et al.*, *Am. J. Cardiol.* **74**, 340 (1994).

12. R. Sassi, *et al.*, *Europace* **17**, 1341 (2015).

13. J. Allen, *Physiol Meas* **28**, 1 (2007).

14. M. Elgendi, *Curr Cardiol Rev* **8**, 14 (2012).

15. A. A. Alian, K. H. Shelley, *Best Pract Res Clin Anaesthesiol* **28**, 395 (2014).

16. N. Pinheiro, *et al.*, *Conf Proc IEEE Eng Med Biol Soc* **2016**, 2945 (2016).

17. V. Jeyhani, S. Mahdiani, M. Peltokangas, A. Vehkaoja, *Conf Proc IEEE Eng Med Biol Soc* **2015**, 5952 (2015).

18. A. Alqaraawi, A. Alwosheel, A. Alasaad, *Healthc Technol Lett* **3**, 136 (2016).

19. W.-H. Lin, D. Wu, C. Li, H. Zhang, Z. Y-T., *The International Conference on Health Informatics* **42**, 213 (2014).

20. N. authors listed, *Eur. Heart J.* **17**, 354 (1996).

21. N. authors listed, *Circulation* **93**, 1043 (1996).

22. F. Shaffer, J. P. Ginsberg, *Front Public Health* **5**, 258 (2017).

23. C. Julien, *Cardiovasc. Res.* **70**, 12 (2006).

24. L. Zhang, *et al.*, *Physiol Meas* **36**, 283 (2015).

25. H. D. Esperer, C. Esperer, R. J. Cohen, *Ann Noninvasive Electrocardiol* **13**, 44 (2008).

26. M. P. Tulppo, T. H. Makikallio, T. Seppanen, J. K. Airaksinen, H. V. Huikuri, *Am. J. Physiol.* **274**, H810 (1998).

27. D. Nunan, G. R. Sandercock, D. A. Brodie, *Pacing Clin Electrophysiol* **33**, 1407 (2010).

28. A. Voss, R. Schroeder, A. Heitmann, A. Peters, S. Perz, *PLoS ONE* **10**, e0118308 (2015).

29. I. M. Irurzun, M. M. Defeo, L. Garavaglia, T. Mailland, E. E. Mola, *arXiv e-prints* p. arXiv:1810.04269 (2018).

30. G. Vandewalle, *et al.*, *J Sleep Res* **16**, 148 (2007).

31. B. Q. Farah, *et al.*, *Pediatr Cardiol* **39**, 466 (2018).

32. R. May, V. McBerty, A. Zaky, M. Gianotti, *J Physiol Anthropol* **36**, 24 (2017).

33. K. L. Rennie, *et al.*, *Am. J. Epidemiol.* **158**, 135 (2003).

34. A. Aubert, *et al.* (1996), vol. 22, pp. 17–20.

35. P. C. Lo, P. H. Tsai, H. J. Kang, W. J. Miao Tian, *J Tradit Complement Med* **9**, 215 (2019).

36. J. R. Krygier, *et al.*, *Int J Psychophysiol* **89**, 305 (2013).

37. S. D. Wu, P. C. Lo, *Biomed. Res.* **29**, 245 (2008).

38. M. Bansal, R. R. Kasliwal, N. Trehan, *Indian Heart J* **66**, 580 (2014).

39. L. G. Goh, T. A. Welborn, S. S. Dhaliwal, *BMC Womens Health* **14**, 118 (2014).

40. C. S. Yoo, K. Lee, S. H. Yi, J. S. Kim, H. C. Kim, *Korean J Fam Med* **32**, 334 (2011).

41. M. Reardon, M. Malik, *Pacing Clin Electrophysiol* **19**, 1863 (1996).

42. U. Zulfiqar, D. A. Jurivich, W. Gao, D. H. Singer, *Am. J. Cardiol.* **105**, 1181 (2010).

Supplementary materials

Data and Methods:

The output of a PPG device is the Interbeat Interval (IBI) tachogram, i.e. the time between peaks of blood volume. The IBI are susceptible to noise due to motion artifacts, electronic noise, missed heart beats, etc. It is essential to clean the IBI field if it is to be a faithful representation of the RR interval tachogram measured by an electrocardiogram (ECG). Cleaning the noisy PPG data is accomplished by a proprietary technique consisting of a median filtering stage, and an anomaly detection stage. Fig. S1 shows the comparison between PPG and ECG, for 60 minutes of data. PPG (with fitbit devices) and ECG (single lead, chest strap) data were simultaneously obtained from ~ 30 subjects (normal sinus rhythm, users were at rest, data was collected with IRB approval). The data was then interpolated so that PPG and ECG readings could be compared at the same instant of time. Fig. S1(a) shows the correlation between the interpolated RR intervals collected by the ECG device, and the interpolated IBI (henceforth IIBI) obtained from PPG. The red points represent raw IIBI, whereas the green dots represent the cleaned IIBI. Fig. S1(b) shows the total power (i.e. power spectrum of the IBI time series data integrated over all frequencies) contained in the data (the power is computed over 5 minute windows). The red points are total power calculations from the raw IIBI, whereas the green points represent total power computed from the cleaned IIBI. For the comparison of total power (plot (b)), the Pearson correlation coefficient between the ECG derived data and the cleaned PPG data is $r = 0.96$, implying a high degree of correlation between PPG derived HRV metrics and ECG derived HRV metrics. In contrast, the correlation is only $r = 0.39$ for the raw data.

It is clear from Fig. S1(b) that cleaning the PPG data is necessary before computing HRV features. Our cleaning algorithm does not make an assumption about noise levels. We define

noise by the prominence, i.e. the value in relation to its neighboring points. Since very noisy samples can affect the prominence, we choose to discard these samples. We discard the data in a time window if the fraction of noise spikes exceeds $\sim 10\%$ of the window size. For the remainder of the paper, we will describe HRV metrics derived from the cleaned PPG data.

We collected data from $\sim$ 8 Million individuals using Fitbit devices over the course of 24 hours. The data was anonymized, and the analysis was consistent with Fitbit's terms and conditions. Table S1 describes the number of individuals in our study, by age and gender. The columns labeled "Fem. (any)" and "Male (any)" are the number of female and male participants with HRV data at some time of the day. The columns labeled (6 am) and (6 pm) show the number of participants with data at 6 am - 7 am and at 6 pm - 7 pm respectively. These times of day are close to the maxima and minima of the HRV circadian rhythm, although these vary by age and gender. We were able to obtain significantly more usable data when the subjects were asleep due to the absence of motion artifacts. Data coverage at 6 am - 7 am for female (male) participants decreases from 70% (65%) for younger users, to 61% (56%) for older users. The coverage at 6 pm - 7 pm for female (male) participants increases from 7.4% (6.6%) to 14% (14%) for older users.

The distribution of HRV metrics is shown in Fig. S2, for subjects of age 30 - 31 yr, for male (green bars) and for female (red bars) participants. The HF power and LF power are strongly skewed, with the mean larger than the median. The RMSSD and Poincare S_1 are also skewed, while the SDRR and Poincare S_2 show a smaller skew. Men have a larger SDRR, LF power, and Poincare S_2 on average compared to women. The difference in gender is less apparent in the RMSSD, HF power, and the Poincare S_1. To estimate the difference in parasympathetic and sympathetic HRV measures between male and female participants, we performed a t-test to quantify the difference as a function of age and time of day. When measured at 6 am - 7 am, the HF power is higher in female subjects for ages $>$ 33 yr, while male subjects have a

higher HF power for smaller ages. When measured at 6 pm - 7 pm, the HF power is higher in female participants for ages > 24 yr. We find that male participants always have higher LF power compared to female participants, but the difference is larger in the morning compared to the evening.

We compute the standard deviation (SDRR) of the IBI, and the root mean squared value of the successive differences (RMSSD), over time windows of size 5 minutes. Time domain HRV metrics are sensitive to the size of the input window since Fourier modes longer than W are not contained in a time window of size W.

Frequency domain calculations require further pre-processing: we resample the IBI field to obtain 512 equally spaced samples in each 5 minute time window. We can thus resolve all frequency components up to $0.5 \times (512/300) \approx 0.85$ Hz. We do not expect significant power at frequencies above 0.5 Hz. The resolution in frequency space is 1/300 Hz which gives us an adequate number of samples in the LF and HF bands. The mean of the data in the time window is subtracted, and the IIBI field is smoothed with a Hann window. A Fast Fourier Transform is then applied to the smoothed IIBI field, and properly normalized to give us the Power Spectral Density (PSD), which is the power contained in the IIBI field per unit frequency. Finally, the PSD is integrated over the relevant frequencies to give us the band power. Frequency domain analysis requires the data in a window to be contiguous and evenly sampled. Therefore, missing data will need to be imputed through interpolation. As a result, we do not consider data windows with a coverage lower than 70%.

Poincare plots are scatter plots obtained by plotting the IBI at time index i against the succeeding IBI, i.e. at time index $i + 1$ (more accurately, these are called first order lag-1 Poincare plots). The Poincare plots will contain a high density of points scattered close to the 45° line. This scatter is a measure of variability. Fig. S3 shows the Poincare plot for a healthy subject. The plot resembles a tapered ellipse since larger IBI allow for more variability. The standard

deviation of points along the major axis (S_2) is a measure of long term variability, while the standard deviation along the minor axis (S_1) is a measure of short term variability.

Table S2, Table S3, and Table S4 show benchmark values for time domain, frequency domain, and graphical domain HRV metrics respectively. The HRV metrics are shown for various ages, for female and male users, and at two times of the day (from 6 am - 7 am, and from 6 pm - 7 pm). We provide the mean, the median, as well as the range from the 25^{th} percentile to the 75^{th} percentile. This range is computed over our entire population for a specific age, gender, and time of day. The measurement from 6 am - 7 am indicates a median over all available 5 minute windows. For a window to be acceptable, the coverage should be adequate, and the noise fraction should be sufficiently small. There are a maximum of 12 such windows in an hour, and we discard the entire hour if there are less than 3 acceptable windows. Table S5 shows the LF/HF ratio which is a measure of sympathovagal balance.

HRV Features - Variation of scaling parameters with age

Metric	Gender		α_0	HRV_0
RMSSD	Female		-0.666	43.7 ms
RMSSD	Male		-0.804	44.8 ms
SDRR	Female		-0.524	54.7 ms
SDRR	Male		-0.566	61.5 ms
HF	Female		-1.480	537.1 ms^2
HF	Male		-1.653	515.6 ms^2
LF	Female		-1.045	917.0 ms^2
LF	Male		-1.006	1195.8 ms^2
S_1	Female		-0.664	32.2 ms
S_1	Male		-0.810	32.6 ms
S_2	Female		-0.337	88.4 ms
S_2	Male		-0.416	98.6 ms

Table 1: The scaling parameters $\alpha_0(g)$ and $HRV_0(g)$

HRV Features - Variation with time of day

Metric	Gender	a_1	a_2	a_3	b_1	b_2	b_3
RMSSD	Female	-0.009	-0.029	-0.003	0.137	0.022	0.001
RMSSD	Male	0.012	-0.02	0.011	0.196	0.035	0.011
SDRR	Female	-0.047	-0.051	0.01	0.173	-0.012	-0.007
SDRR	Male	-0.052	-0.044	0.019	0.2	-0.01	-0.001
HF	Female	-0.02	-0.06	0.025	0.323	0.015	-0.02
HF	Male	0.021	-0.046	0.033	0.382	0.044	0.005
LF	Female	-0.06	-0.098	0.022	0.317	-0.014	-0.016
LF	Male	-0.067	-0.073	0.043	0.335	-0.015	-0.004
S1	Female	-0.035	-0.05	0.003	0.137	-0.010	-0.015
S1	Male	0.007	-0.03	0.009	0.181	0.0130	0.0
S2	Female	-0.063	-0.061	0.010	0.170	-0.002	-0.002
S2	Male	-0.059	-0.056	0.009	0.193	0.014	0.007

Table 2: Variation of time dependent scaling parameters: The first 3 Fourier components.

Variation of HRV metrics with activity

Gender	Metric	Age (yr)	r	C (ms^2)	σ (steps)
Male	HF	20-24	0.961	865	32
Female	HF	20-24	0.985	873	30
Male	LF	20-24	0.946	1758	25
Female	LF	20-24	0.973	1314	20
Male	HF	50-54	0.859	234	295
Female	HF	50-54	0.954	254	195
Male	LF	50-54	0.969	683	42
Female	LF	50-54	0.979	510	48

Table 3: Effect of activity on HRV power. People of all ages can improve their HRV through physical activity, but the effect is larger for younger users, especially for HF power.

User distribution by age and gender

Age	Fem.	Fem.	Fem.	Male	Male	Male
(yr)	(any)	(6 am)	(6 pm)	(any)	(6 am)	(6 pm)
< 20	168k	118k	12k	69k	45k	5k
20-30	895k	598k	84k	340k	217k	32k
30-40	1.23M	811k	114k	582k	360k	54k
40-50	1.16M	748k	131k	593k	359k	65k
50-60	1.06M	651k	134k	570k	333k	72k
60-70	688k	417k	96k	406k	231k	56k
> 70	248k	150k	36k	188k	105k	27k

Table S1: Number of participants in the present study, by age and gender. The amount of data depends on the time of day since we lose data during the daytime due to motion artifacts.

HRV Features - Time Domain

Time of day	Age	RMSSD (female)			RMSSD (male)			SDRR (female)			SDRR (male)		
	(yr)	(mean)	(med)	(25p-75p)	(mean)	(med)	(25p-75p)	(mean)	(med)	(25p-75p)	(mean)	(med)	(25p-75p)
6am - 7am	20	66	56	37 - 85	74	66	45 - 96	81	76	56 - 101	91	88	66 - 114
6am - 7am	25	57	48	32 - 73	61	54	35 - 79	73	68	50 - 91	82	79	57 - 103
6am - 7am	30	53	45	31 - 67	56	49	34 - 71	69	65	49 - 86	79	75	57 - 98
6am - 7am	35	47	41	29 - 60	49	43	31 - 62	64	61	46 - 79	73	70	54 - 91
6am - 7am	40	42	37	26 - 52	43	38	27 - 54	59	56	43 - 73	68	65	50 - 85
6am - 7am	45	37	33	24 - 46	38	34	25 - 48	54	51	40 - 66	64	61	47 - 78
6am - 7am	50	34	31	22 - 42	34	31	23 - 42	51	49	38 - 63	59	56	42 - 72
6am - 7am	55	33	29	22 - 40	32	29	21 - 39	49	47	36 - 61	55	52	40 - 68
6am - 7am	60	31	28	21 - 38	31	27	20 - 37	46	44	34 - 57	52	49	37 - 64
6pm - 7pm	20	49	41	28 - 62	53	45	30 - 66	58	54	40 - 73	66	63	46 - 82
6pm - 7pm	25	41	34	24 - 51	41	34	23 - 53	51	46	35 - 63	55	52	37 - 70
6pm - 7pm	30	40	34	24 - 50	38	33	23 - 47	49	46	35 - 60	54	51	39 - 67
6pm - 7pm	35	36	31	22 - 44	34	29	21 - 42	45	42	32 - 55	49	46	35 - 60
6pm - 7pm	40	33	29	21 - 40	30	26	19 - 37	41	39	30 - 50	45	42	32 - 55
6pm - 7pm	45	31	27	20 - 38	27	24	18 - 34	38	36	28 - 46	41	39	30 - 51
6pm - 7pm	50	29	26	19 - 35	25	22	16 - 31	36	35	27 - 44	38	36	27 - 46
6pm - 7pm	55	27	25	18 - 33	24	21	16 - 29	34	33	26 - 42	35	33	25 - 43
6pm - 7pm	60	26	24	18 - 32	24	21	15 - 28	32	30	24 - 39	34	31	24 - 41

Table S2: Typical values for time domain HRV features: The RMSSD distribution is more skewed than the SDRR distribution (see Fig. S2) and this is reflected in the difference between the mean and the median. Bin size for the age is 1 year, i.e. age = 20 includes users between 20 and 21 years of age.

HRV Features - Frequency Domain

Time of day	Age		HF (female)			HF (male)			LF (female)			LF (male)		
	(yr)		(mean)	(med)	(25p-75p)	(mean)	(med)	(25p-75p)	(mean)	(med)	(25p-75p)	(mean)	(med)	(25p-75p)
6am - 7am	20		1311	759	359 - 1566	1352	868	448 - 1665	1875	1372	737 - 2395	2265	1749	991 - 2925
6am - 7am	25		971	543	250 - 1147	970	582	269 - 1169	1568	1120	570 - 2014	1954	1486	779 - 2551
6am - 7am	30		822	474	232 - 962	779	488	251 - 922	1418	1018	547 - 1798	1816	1406	793 - 2341
6am - 7am	35		657	375	189 - 749	599	375	195 - 710	1209	859	471 - 1530	1600	1227	694 - 2055
6am - 7am	40		497	290	150 - 567	464	286	151 - 543	1015	721	397 - 1282	1389	1048	588 - 1788
6am - 7am	45		379	225	118 - 432	366	221	118 - 411	842	593	331 - 1048	1176	876	490 - 1502
6am - 7am	50		313	190	101 - 356	283	171	92 - 317	728	508	288 - 893	990	709	392 - 1242
6am - 7am	55		280	170	91 - 314	245	138	75 - 255	659	450	254 - 794	853	586	321 - 1033
6am - 7am	60		251	146	79 - 270	243	116	64 - 214	576	374	210 - 670	759	469	259 - 858
6pm - 7pm	20		698	359	167 - 781	710	397	188 - 803	1071	733	394 - 1343	1339	999	538 - 1681
6pm - 7pm	25		478	235	108 - 515	436	214	90 - 482	820	524	273 - 1015	1035	690	331 - 1312
6pm - 7pm	30		419	214	106 - 445	381	192	97 - 400	761	504	279 - 924	971	698	390 - 1232
6pm - 7pm	35		327	173	87 - 348	285	145	73 - 292	628	418	231 - 749	809	558	310 - 1012
6pm - 7pm	40		254	142	75 - 270	216	112	58 - 225	524	351	199 - 612	675	457	246 - 831
6pm - 7pm	45		213	119	63 - 223	172	93	48 - 175	440	293	167 - 508	557	375	202 - 673
6pm - 7pm	50		184	104	55 - 192	136	74	39 - 139	383	254	145 - 446	455	302	164 - 540
6pm - 7pm	55		160	90	49 - 165	129	63	34 - 116	334	221	125 - 380	386	244	131 - 437
6pm - 7pm	60		143	79	44 - 145	135	57	32 - 106	292	186	107 - 325	358	204	110 - 373

Table S3: Typical values for frequency domain HRV features. Presented are mean, median, and the range from the 25^{th} to the 75^{th} percentile, across gender and age ranges. Similar to Table S2, the HRV values vary significantly with time of day.

HRV Features - Graphical Domain

Time of day	Age	Poincare S_1 (female)			Poincare S_1 (male)			Poincare S_2 (female)			Poincare S_2 (male)		
	(yr)	(mean)	(med)	(25p-75p)	(mean)	(med)	(25p-75p)	(mean)	(med)	(25p-75p)	(mean)	(med)	(25p-75p)
6am - 7am	20	50	43	27 - 66	56	51	34 - 72	120	115	84 - 148	141	134	103 - 171
6am - 7am	25	43	37	23 - 57	45	40	25 - 59	113	107	77 - 141	128	121	86 - 160
6am - 7am	30	40	35	22 - 52	40	36	23 - 53	112	106	77 - 137	125	116	83 - 154
6am - 7am	35	37	31	21 - 46	35	31	20 - 45	109	101	73 - 134	120	109	77 - 149
6am - 7am	40	33	28	19 - 41	31	27	18 - 40	104	96	70 - 127	115	104	72 - 143
6am - 7am	45	29	25	17 - 36	28	24	16 - 35	99	91	66 - 122	112	99	69 - 140
6am - 7am	50	27	23	16 - 33	25	21	15 - 30	98	89	64 - 122	105	92	64 - 131
6am - 7am	55	25	22	15 - 30	24	20	14 - 28	98	87	63 - 121	104	90	63 - 129
6am - 7am	60	24	21	15 - 29	25	19	14 - 27	95	84	60 - 118	103	89	62 - 131
6pm - 7pm	20	37	31	20 - 46	39	32	20 - 49	90	83	61 - 109	102	93	70 - 127
6pm - 7pm	25	31	25	17 - 37	30	23	15 - 37	82	74	54 - 100	90	81	59 - 113
6pm - 7pm	30	30	24	17 - 36	29	24	16 - 34	81	74	54 - 100	91	84	62 - 110
6pm - 7pm	35	27	23	16 - 32	26	21	14 - 30	77	70	52 - 93	83	76	55 - 103
6pm - 7pm	40	24	21	15 - 28	22	18	13 - 26	71	64	48 - 87	76	69	50 - 94
6pm - 7pm	45	23	20	14 - 27	20	17	12 - 23	68	62	46 - 83	72	65	47 - 88
6pm - 7pm	50	21	18	13 - 25	18	15	11 - 21	64	58	44 - 77	67	60	45 - 83
6pm - 7pm	55	20	17	13 - 23	18	14	11 - 20	63	57	42 - 76	64	57	43 - 79
6pm - 7pm	60	19	16	12 - 22	18	14	10 - 19	61	54	41 - 74	61	55	40 - 75

Table S4: Typical HRV values for graphical domain Poincare S_1 and S_2 features. Similar to Tables S2 and S3, presented are mean, median, and the range from the 25^{th} to the 75^{th} percentile, across gender and age ranges.

HRV Features - Sympathovagal balance

Time of day	Age		LF / HF (female)			LF / HF (male)		
	(yr)		(mean)	(med)	(25p-75p)	(mean)	(med)	(25p-75p)
6am - 7am	20		2.175	1.765	1.124 - 2.748	2.505	2.007	1.239 - 3.170
6am - 7am	25		2.486	2.004	1.258 - 3.149	3.207	2.500	1.504 - 4.097
6am - 7am	30		2.608	2.091	1.313 - 3.316	3.547	2.827	1.744 - 4.560
6am - 7am	35		2.798	2.230	1.391 - 3.558	3.991	3.198	1.951 - 5.116
6am - 7am	40		3.045	2.431	1.513 - 3.870	4.432	3.583	2.164 - 5.744
6am - 7am	45		3.257	2.593	1.602 - 4.135	4.819	3.877	2.359 - 6.230
6am - 7am	50		3.378	2.674	1.650 - 4.281	5.125	4.103	2.508 - 6.608
6am - 7am	55		3.351	2.641	1.625 - 4.257	5.202	4.148	2.509 - 6.708
6am - 7am	60		3.282	2.581	1.572 - 4.164	5.071	4.021	2.404 - 6.534
6pm - 7pm	20		2.441	2.021	1.260 - 3.117	3.000	2.480	1.579 - 3.801
6pm - 7pm	25		2.653	2.208	1.401 - 3.371	3.840	3.141	1.953 - 4.952
6pm - 7pm	30		2.794	2.334	1.487 - 3.544	4.228	3.545	2.218 - 5.511
6pm - 7pm	35		2.887	2.385	1.544 - 3.705	4.547	3.845	2.467 - 5.817
6pm - 7pm	40		2.971	2.471	1.595 - 3.770	4.794	4.003	2.550 - 6.118
6pm - 7pm	45		2.970	2.471	1.592 - 3.716	4.785	4.000	2.504 - 6.078
6pm - 7pm	50		2.970	2.500	1.607 - 3.729	4.871	4.028	2.524 - 6.203
6pm - 7pm	55		2.913	2.409	1.571 - 3.677	4.623	3.803	2.360 - 5.917
6pm - 7pm	60		2.815	2.313	1.512 - 3.521	4.287	3.482	2.165 - 5.504

Table S5: Sympathovagal balance: The LF/HF ratio is the estimate of the relative strengths of the sympathetic and parasympathetic branches. Presented are mean, median, and the range from the 25^{th} to the 75^{th} percentile, across gender and age ranges.

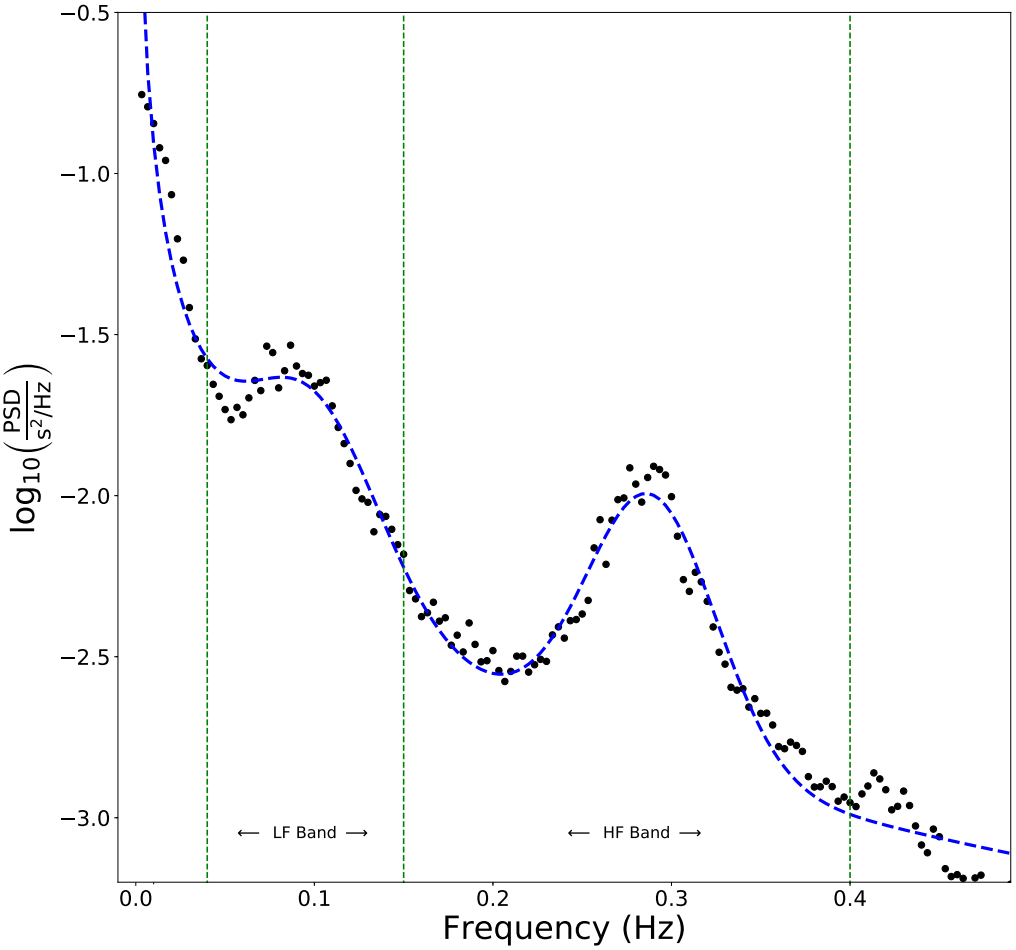

Figure 1: Power Spectral Density measured for a single individual over one night, showing 2 features: The Mayer wave centered at 0.0975 Hz corresponding to arterial blood pressure oscillations with a timescale of 10.3 s, and sinus arrhythmia due to respiration centered at 0.288 Hz implying a respiration rate of 17.3 breaths per minute.

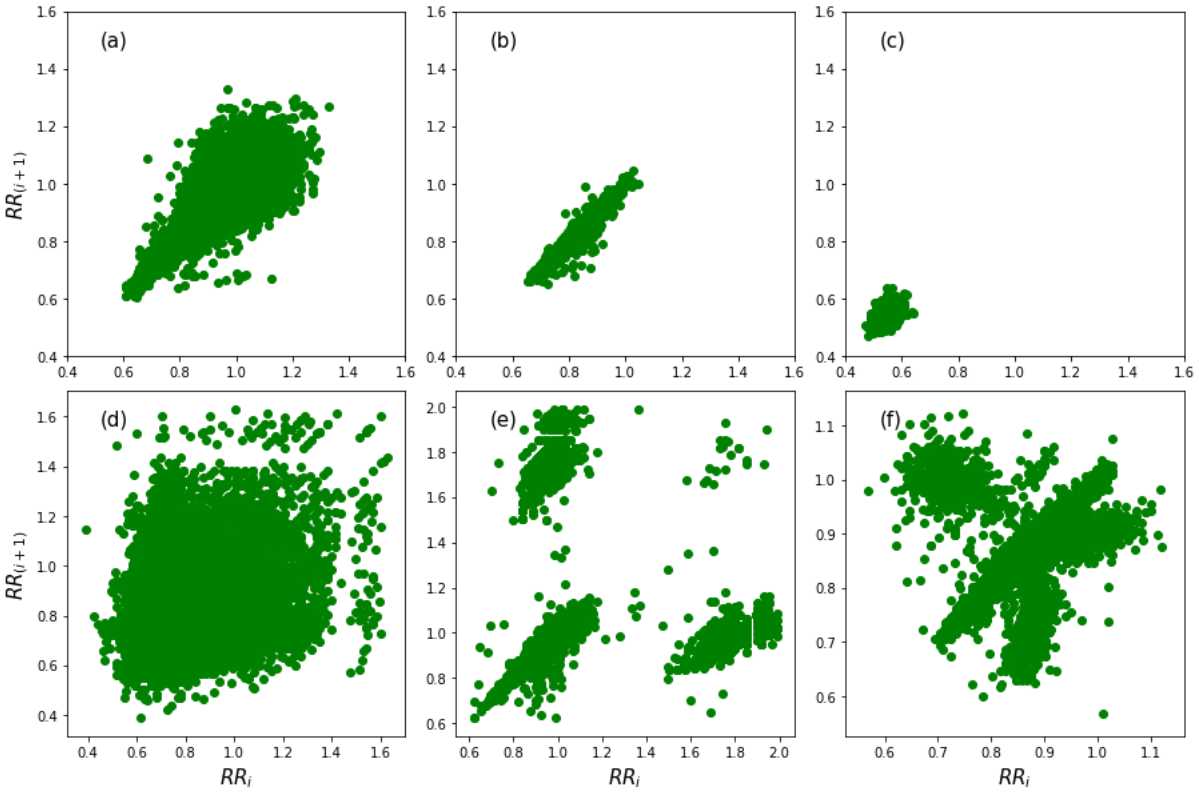

Figure 2: Poincare plots are very useful in diagnosing heart arrhythmias. (a) shows the "comet" pattern of a healthy heart. (b) shows the "torpedo" pattern indicating low short term variability. (c) is an example of a heart in tachycardia. (d) shows the fan pattern suggestive of atrial fibrillation. (e) and (f) show bi-lobed and tri-lobed patterns which could indicate premature atrial and ventricular contractions.

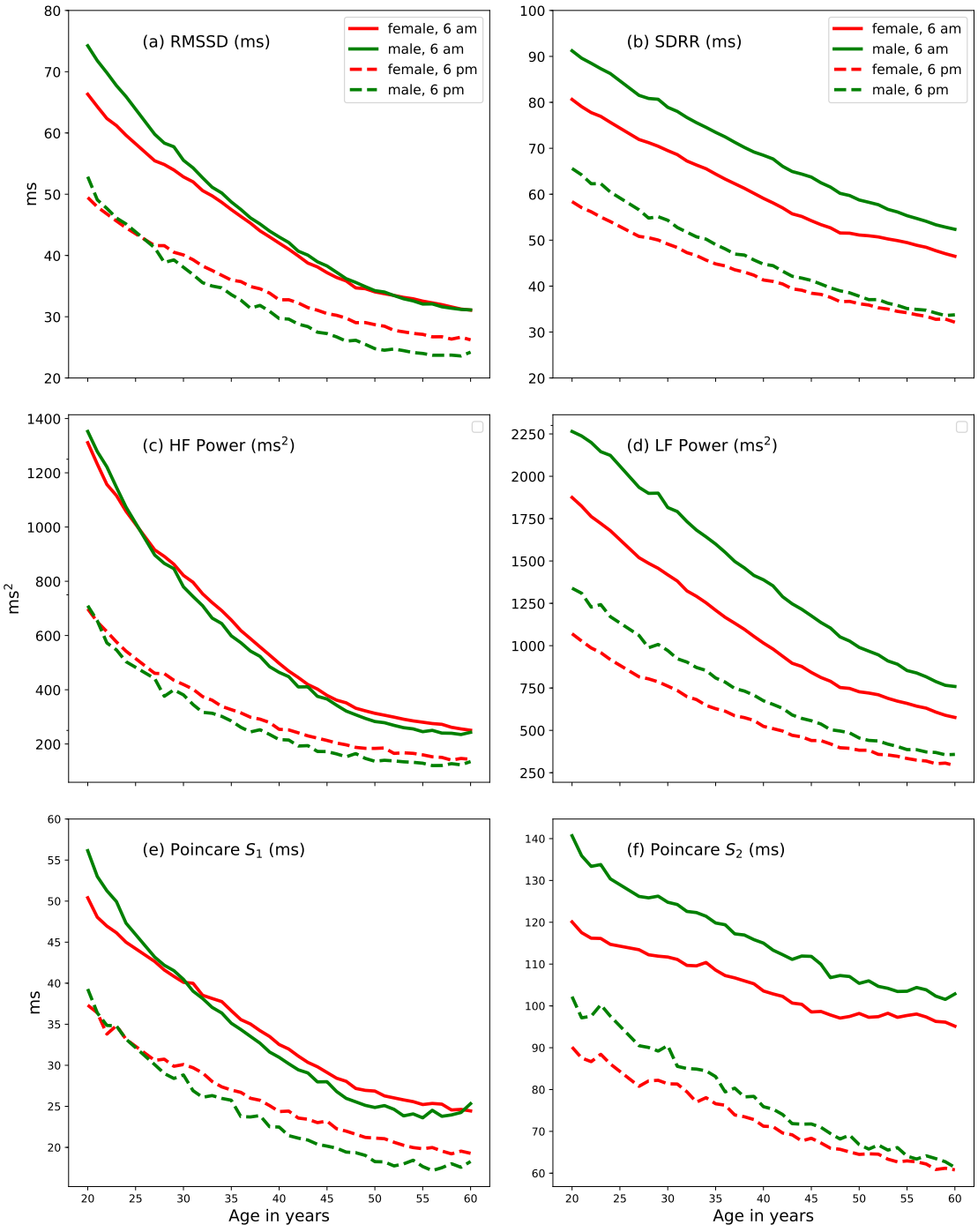

Figure 3: Decline in HRV with age. All metrics decrease with age, for both men and women. However, the parasympathetic measures (RMSSD, HF power, and Poincare S_1) decline faster than the sympathetic measures (SDRR, LF power, and Poincare S_2).

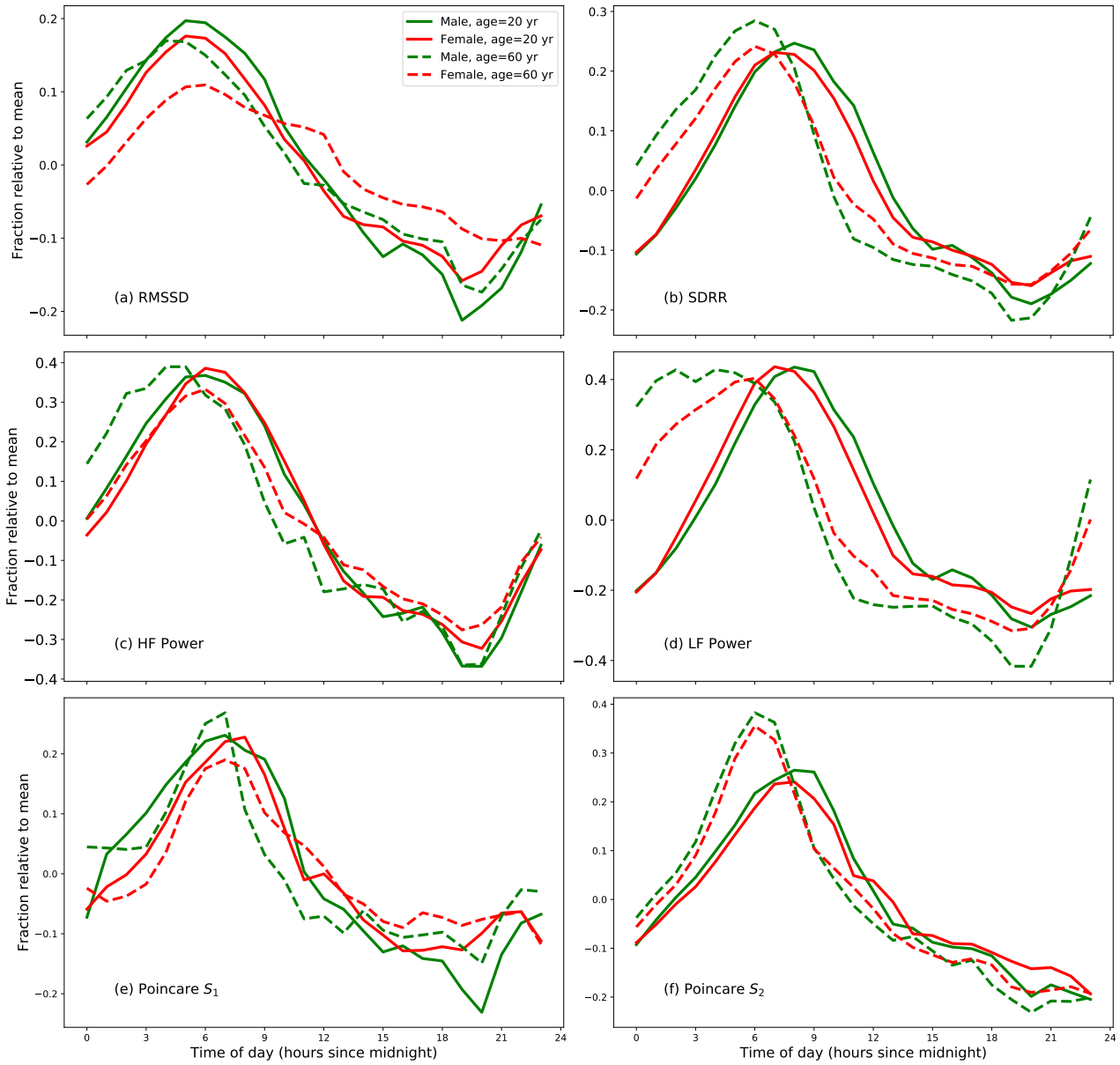

Figure 4: Daily variation of HRV features. The modulation is substantial for all ages. The phase of the sympathetic measures (i.e. SDRR, LF power, and Poincare S_2) shifts to earlier times for older individuals. The change in phase with age is less prominent in the modulation of the parasympathetic measures (RMSSD, LF power, and Poincare S_1).

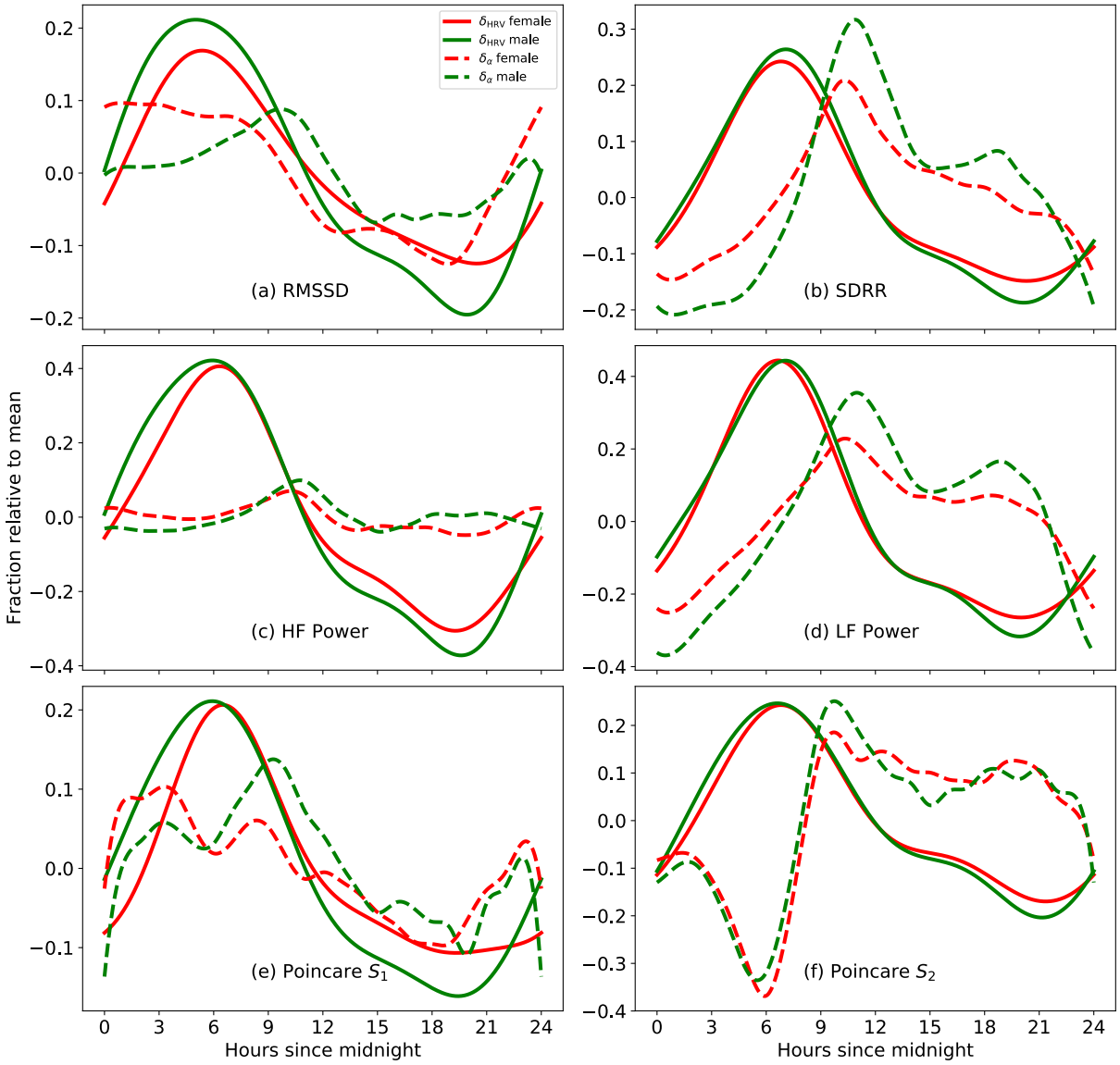

Figure 5: Daily variation of the time dependent scaling parameters: δ_{H} and δ_{α}. The variation of δ_{α} is larger for the sympathetic measures (SDRR, LF power, Poincare S_2) compared to the parasympathetic measures (RMSSD, HF power, Poincare S_1). This helps explain the change in phase seen in Fig. 4

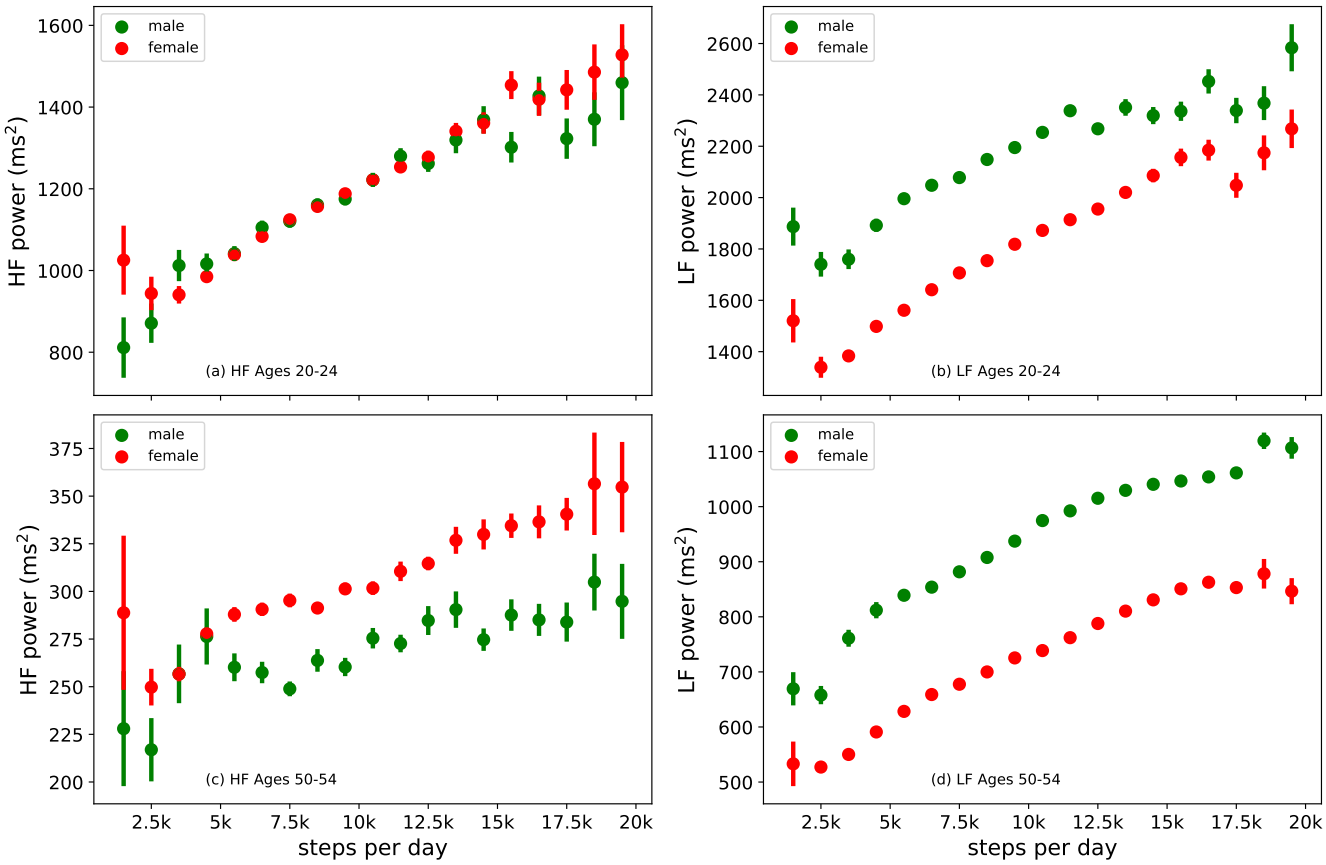

Figure 6: HRV can be increased with physical exercise for all ages, but especially for younger individuals. Shown are HF and LF variations (measured from 6 am - 7am) with the number of steps per day, for young (ages 20-24 yr) and older (ages 50-54 yr) participants.

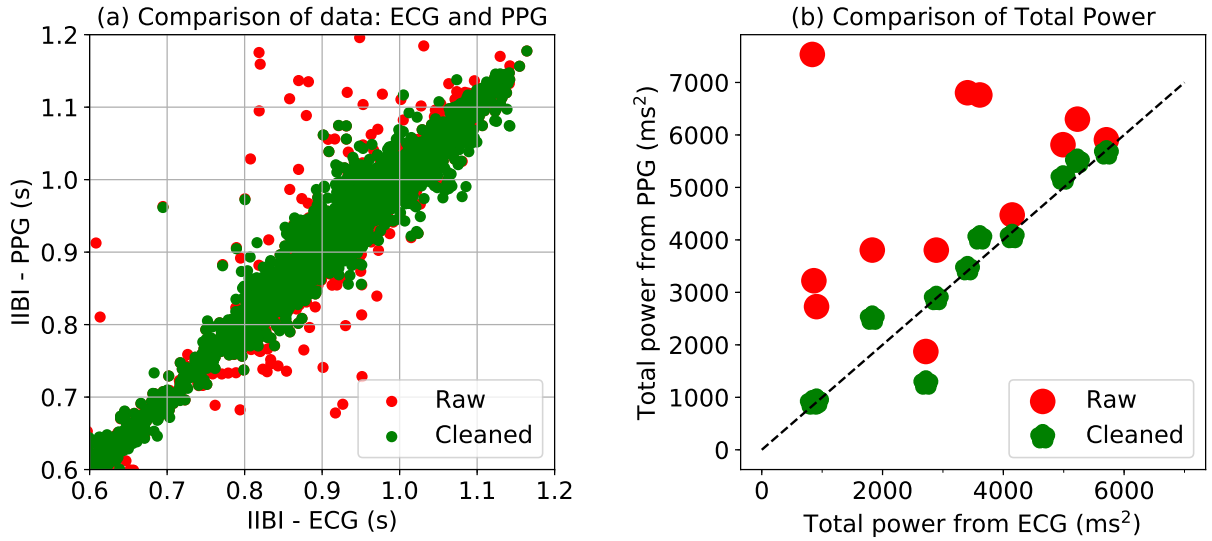

Figure S1: Comparison of PPG and ECG: Data is simultaneously obtained from subjects using PPG and ECG. The data is then interpolated so as to obtain data points at exactly the same time. (a) show the correlation between the ECG derived interpolated RR intervals and the PPG derived interbeat intervals (IBI). (b) shows the correlation between the total power obtained from the interpolated RR tachogram and the total power obtained from the interpolated IBI.

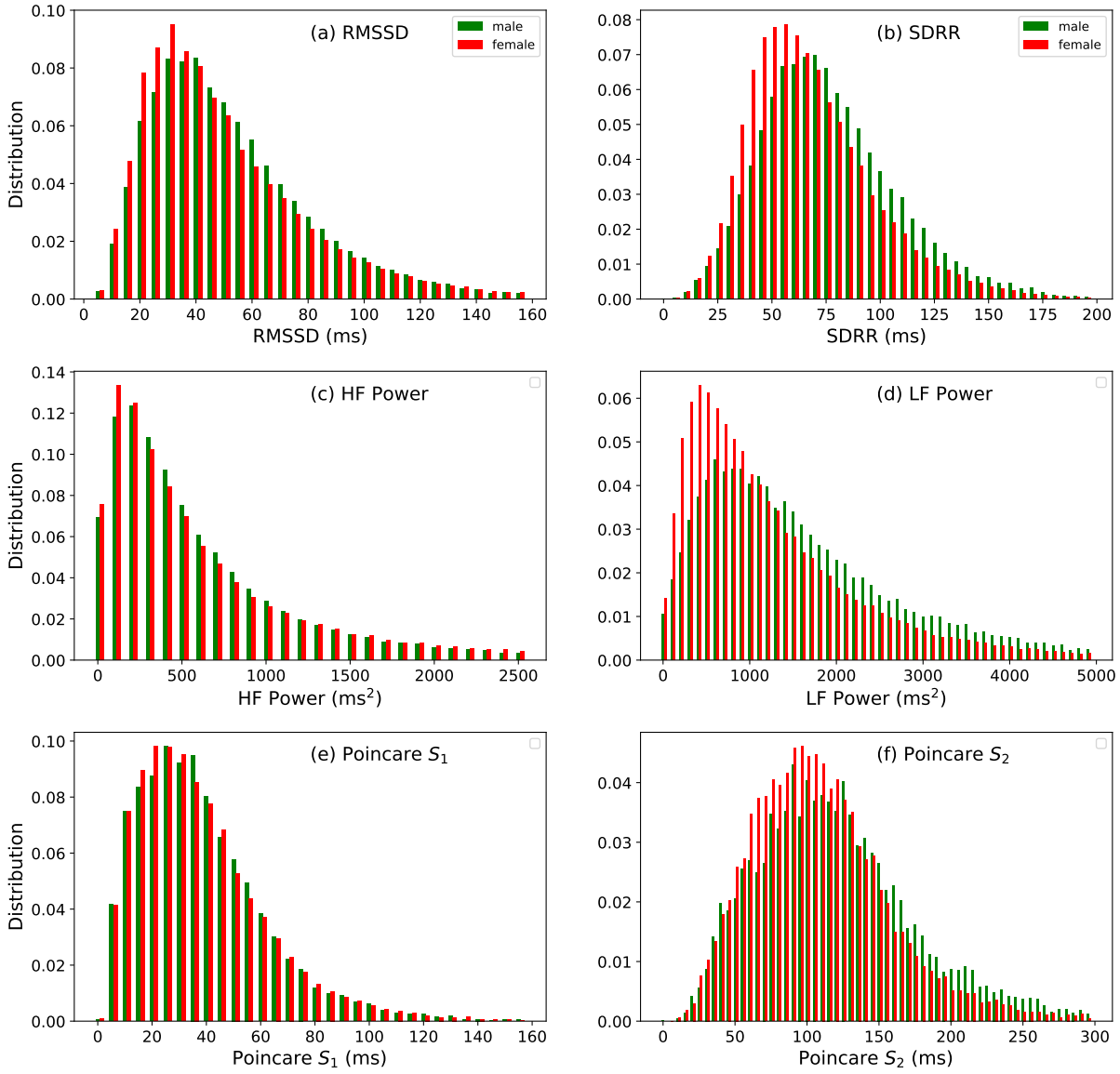

Figure S2: The distribution of HRV metrics for individuals in the age range 30 - 31 yr. The indicators of parasympathetic function namely, the RMSSD, HF power, and Poincare S_1 distributions are similar, and show little variation with gender. On the other hand, men have higher SDRR, LF power, and Poincare S_2 on average, compared to women, which indicates higher sympathetic activity.

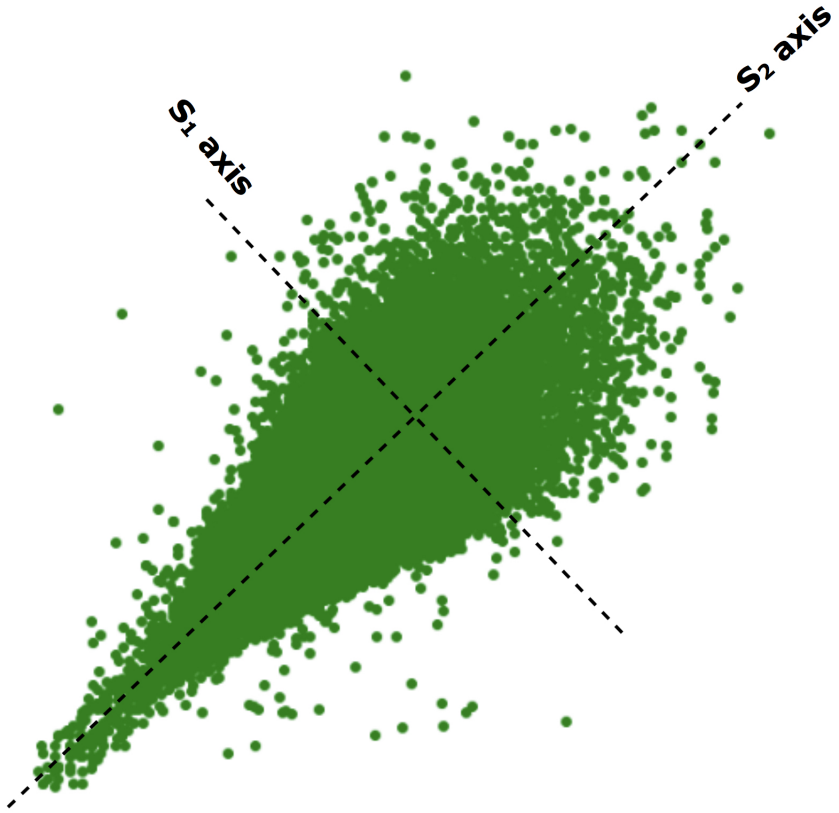

Figure S3: Poincare scatter plot: IBI at time index i plotted against the IBI at time index $(i+1)$. The Poincare plot resembles a tapered ellipse since the variability is larger for large values of IBI.